Charge Order and Tilt Modulation in Multiferroic $K_xM^{II}_xM^{III}_{1-x}F_3$ ($0.4 < x < 0.6$) Transition Metal Fluorides with Tetragonal Tungsten Bronze Structure

Simone Fabbrici,[†] Erica Montanari,[†] Lara Righi,[†] Gianluca Calestani,*[,†] and Andrea Migliori[‡]

Dipartimento di Chimica GIAF, Università di Parma, Parco Area delle Scienze 17A, I-43100 Parma, Italy, and CNR-IMM, Sezione di Bologna, Via Gobetti 101, I-40126 Bologna, Italy

Received April 22, 2004. Revised Manuscript Received May 27, 2004

Transition metal fluorides with tetragonal tungsten bronze (TTB) structure, having general formula $K_xM^{II}_xM^{III}_{1-x}F_3$ with $0.4 < x < 0.6$ and M belonging to transition metals, have been studied over the past decades because of the frustrated magnetic ordering arising at low temperature. We investigated the structural properties of TTB fluorides by transmission electron microscopy (TEM). The results, coupled with an accurate structure analysis performed by single-crystal XRD on $K_{0.53}FeF_3$, revealed ferroelectricity and a unified structural description of these materials, where charge order and tilt modulations coexist, each one with its own periodicity differently commensurate to the conventional TTB cell. Whereas the charge order is peculiar of the mixed valence fluorides, the nature of the tilt modulation is clearly associable to the structural features of TTB niobates, suggesting also for the fluoride bronzes the existence of a generalized ferroelectric-ferroelastic behavior at room temperature.

Introduction

The term "tetragonal tungsten bronze" (TTB), originally utilized to indicate the nonstoichiometric compound K_xWO_3 ($x = 0.4-0.6$), was successively extended to all the compounds showing a similar structure. The TTB family, whose extension has considerably increased with time by substituting tungsten with other high valence transition metals and potassium with Li, Na, Ba, Sr, and Pb ions, groups today a large number of functional crystals and materials possessing electrooptic, ferroelectric, pyroelectric, and piezoelectric properties. Among these, particular importance have assumed the ferroelectric niobates, crystallizing in variants of the tetragonal tungsten bronze structure,[1] which represent a very interesting class of materials for device application because of a large nonlinear polarizability that is at the basis of useful electrooptical and nonlinear optical properties. For example $Ba_2NaNb_5O_{15}$ (BNN), which represents a prototype for over 150 individual end-member bronze compositions and all their possible solid solutions,[2] is a well-known and extremely efficient second harmonic generator stable to focused laser radiation at 488 nm.[3] By making use of these properties, continuous parametric oscillators tunable over a wide frequency range have been constructed.[4]

By substituting oxygen with fluorine, the TTB structure becomes accessible to lower valence transition metals. Fluorides with TTB structure, having the general formula $K_xM^{II}_xM^{III}_{1-x}F_3$, $0.4 < x < 0.6$, were first reported by De Pape[5] in 1965. The TTB phase has been reported to form in V(II)/V(III),[6] Fe(II)/Fe(III),[5] Co(II)/Fe(III),[7] Mn(II)/Fe(III),[8] Mn(II)/Cr(III),[9] and Mg/In[10] systems and its structural stability has been found to critically depend on the size of the M^{II} and M^{III} species.[11] A complete study on the influence of the K/M ratio on the formation of different fluoride bronzes has been published only for the Fe(II)/Fe(III) system.[11,12] TTB fluorides have been extensively studied because of the frustrated magnetic ordering[7,9,13−17] which arises at low temperature. The existence of ferroelectricity in TTB

* To whom correspondence should be addressed. Tel: +390521905447. Fax: +390521905556. E-mail: calestg@unipr.it.
[†] Università di Parma.
[‡] CNR-IMM, Sezione di Bologna.

(1) Jamieson, P. B.; Abrahams S. C.; Bernstein, J. L. *J. Chem. Phys.* **1968** *48*, 5048.
(2) Sambasiva Rao, K.; Hyun Yoon, K. *J. Mater. Sci.* **2003**, *38*, 391.
(3) Geusic, J. E.; Levinstein, H. J.; Singh, S.; Smith, R. G.; Van Uitert, L. G. *Appl. Phys. Lett.* **1968**, *12*, 306.
(4) Smith, R. G.; Geusic, J. E.; Levinstein, H. J.; Rubin, J. J.; Singh, S.; Van Uitert, L. G. *Appl. Phys. Lett.* **1968**, *12*, 308.
(5) De Pape, R. *C. R. Acad. Sci. Paris* **1965**, *260*, 4527.
(6) Williamson, R. F.; Boo, W. O. *J. Inorg. Chem.* **1977**, *16*, 649.
(7) Giri, S.; Ghoshray, K. *Phys. Rev. B* **1998**, *57*, 5918.
(8) Banks, E.; Nakajima, S.; Williams, G. J. B. *Acta Crystallogr., Sect. B: Struct. Sci.* **1979**, *35*, 46.
(9) Banks, E.; Shone, M.; Hong, Y. S.; Williamson, R. F.; Boo, W. O. *J. Inorg. Chem.* **1982**, *21*, 3894.
(10) Caramanian, A.; Dupont, N.; Gredin, P.; de Kozak, A. *Z. Anorg. Allg. Chem.* **1999**, *625*, 933.
(11) Ferey, G. Ph.D. Thesis, Université Pierre et Marie Curie (Paris VI) 1977.
(12) Tressaud, A.; De Pape, R.; Portier, J.; Hagenmuller, P. *Bull. Soc. Chim. France* **1970**, *10*, 3411.
(13) Banks, E.; Shone, Y. S.; Williamson, R. F.; Boo, W. O. *J. Inorg. Chem.* **1983**, *22*, 3339.
(14) Lacorre, P.; Pannetier, J.; Ferey, G. *J. Magn. Magn. Mater.* **1991**, *94* 331.
(15) Giri, S.; Ghoshray, K.; Ghoshray, A.; Chatterjee, N. *J. Magn. Magn. Mater.* **1996**, *157*, 411.
(16) Mohammad Yusuf, Sk.; Madhav Rao, L.; Mukhopadhyay, R.; Giri, S.; Ghoshray, K.; Ghoshray, A. *Solid State Commun.* **1997**, *101*, 145.

10.1021/cm049346p CCC: $27.50
Published on Web 07/10/2004

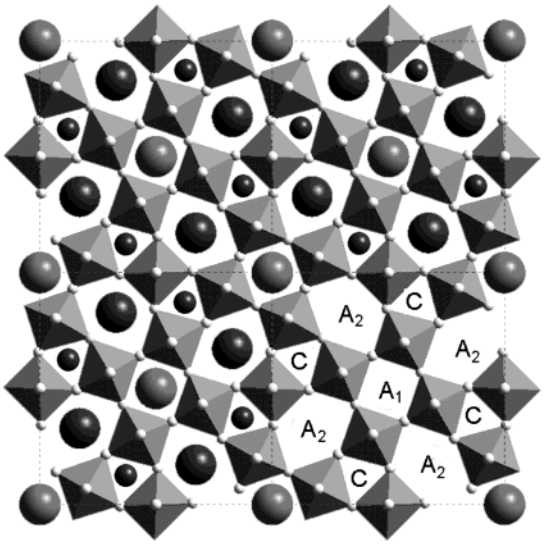

Figure 1. Drawing of TTB structure with the conventional sites nomenclature.

fluorides has been reported for the composition $K_{0.6}FeF_3$, and it has been related to orthorhombic distortion of TTB cell.[18,19] The possible coexistence of electric and magnetic ordering in TTB fluorides makes these materials potential multiferroic systems.

The tetragonal tungsten bronzes are layered structures characterized by the structural formula $(A_1)_x(A_2)_y$-$C_zB_{10}X_{30}$, where x can ideally vary in the range 0−2 and y and z are in the range 0−4. Their typical structure framework (Figure 1), which can be thought of as derived from the perovskite structure by rotation of some $[BX_6]$ octahedra, is formed by corner sharing of the $[BX_6]$ units, whose linking produces three different types of channels (also called tunnels) containing the alkaline cations in A_1, A_2, and C sites, respectively. In terms of coordination polyhedra, A_2 cations are 15-fold coordinated in the tunnel with a pentagonal section, A_1 cations are 12-fold coordinated in the surviving perovskite cage, and C cations are 9-fold coordinated in channels characterized by a triangular section. The C site is empty in fluoride bronzes, being too small to host the potassium cation.

Despite different structural characterizations, mostly performed by X-ray powder diffraction, that agree in assigning to these fluorides the typical TTB structure or related variants, detailed quantitative structural studies of TTB fluorides are quite rare. Published works based on single-crystal XRD data considered the compositions $K_{0.6}FeF_3$,[20] $K_{0.54}(Mn,Fe)F_3$,[8] and $K_{0.38}Mg_{0.38}$-$In_{0.62}F_3$.[10] The crystal structure of $K_{0.6}FeF_3$ was reported to consist of a slightly distorted TTB cell having orthorhombic symmetry, with lattice parameters $a = 12.637$, $b = 12.750$, and $c = 3.986$ Å and space group *Pba2*. On the basis of the interatomic distances, Fe^{2+} and Fe^{3+} were found to be mostly random distributed in the structure, with the exception of the extra-perovskite site (the one linking four different perovskite units), which is preferentially occupied by Fe^{3+}. Further Mössbauer studies, although revealing the presence of cationic order, were unable to univocally determine its nature.[11,21] In contrast, $K_{0.54}(Mn,Fe)F_3$ was found to be tetragonal, space group $P4_2bc$. Its cell (lattice parameters $a = 12{,}765$ Å and $c = 8{,}002$ Å) shows a doubling of the c axis with respect to the conventional TTB structure, which is produced by the ordering of Mn^{2+} and Fe^{3+} cations. They are stacked in an alternate way around the perovskite cage and along the c axis, whereas the extra-perovskite site is occupied in a disordered way. A similar pseudotetragonal cell, showing monoclinic $P2_1/a$ symmetry, was reported also for $K_{0.38}Mg_{0.38}In_{0.62}F_3$. Differently from the previous case, no cationic order was found and the doubling of the c axis was attributed to the alternate tilting, along the c direction, of the rows of $[MF_6]$ octahedra. Differently from the first two structures, the last one is centrosymmetric and therefore is not consistent with the ferroelectric behavior which is typical of several TTB bronzes. However it must be noticed that, as far as fluorides are concerned, ferroelectricity has been reported only for $K_{0.6}FeF_3$ and mostly attributed to the orthorhombic distortion of its structure.

These few structural works draw divergent conclusions for the existence of cationic ordering as well as the origin of the observed superstructure. Cationic order was not observed in Mg/In based fluoride, but it was found in Fe and Fe/Mn based bronzes, where, however, the ordering mechanism differs completely. Such a difference between the two last compounds cannot be justified easily by the change in the chemical composition, as metal ions share the same valence, and ionic radii of bivalent iron and manganese ions are similar. A superstructure related to the doubling of the c axis of the conventional TTB structure was observed for both Fe/Mn and Mg/In based bronzes, but attributed to cationic ordering in one case and to cooperative tilt of the $[MF_6]$ octahedra in the other. Because the existence of a tilt modulation is a characteristic structural feature of tungsten bronze niobates, where it has been put in evidence in particular by electron diffraction (ED) studies, we investigated the structural properties of TTB fluorides by transmission electron microscopy (TEM). The results, coupled with an accurate structure analysis performed by single-crystal XRD on $K_{0.53}FeF_3$, are presented in this paper and reveal a unified structural description of these materials, where charge order and tilt modulations coexist, each one with its own periodicity differently commensurate to the conventional TTB cell.

Experimental Section

A series of fluorides with nominal compositions $K_{0.4}M^{II}_{0.4}$-$M^{III}_{0.6}F_3$ and $K_{0.6}M^{II}_{0.6}M^{III}_{0.4}F_3$, where M^{II} = Fe, Mn, Co or a mixture thereof and M^{III} = Fe, Mn, Cr, In or a mixture thereof, were prepared by solid state reaction. Stoichiometric quantities of elementary fluorides (Aldrich Chemicals), were carefully mixed and ground, mechanically sealed in Ag tubes, and fired under nitrogen atmosphere at 700 °C for a time ranging from 12 to 24 h. The reactions generally returned powder products, but in some cases single crystals suitable for XRD analysis could be isolated from the reacted mass.

(17) Bhargava, S. C.; Singh, S.; Moffish, A. H.; Li, Z. W. *Solid State Commun.* **2000**, *116*, 575.
(18) Ravez, J.; Abrahams, S. C.; De Pape, R. *J. Appl. Phys.* **1989**, *65*, 3987.
(19) Ravez, J.; Abrahams, S. C.; Mercier, A. M.; Rabardel, L.; De Pape, R. *J. Appl. Phys.* **1990**, *67*, 2681.
(20) Hardy, A. M.; Hardy, A.; Ferey, G. *Acta Crystallogr., Sect. B: Struct. Sci.* **1973**, *29*, 1654.
(21) Ferey, G.; De Pape, R.; Varret, F. *J. Phys., Colloq.* **1977**, *38*, C7−107.

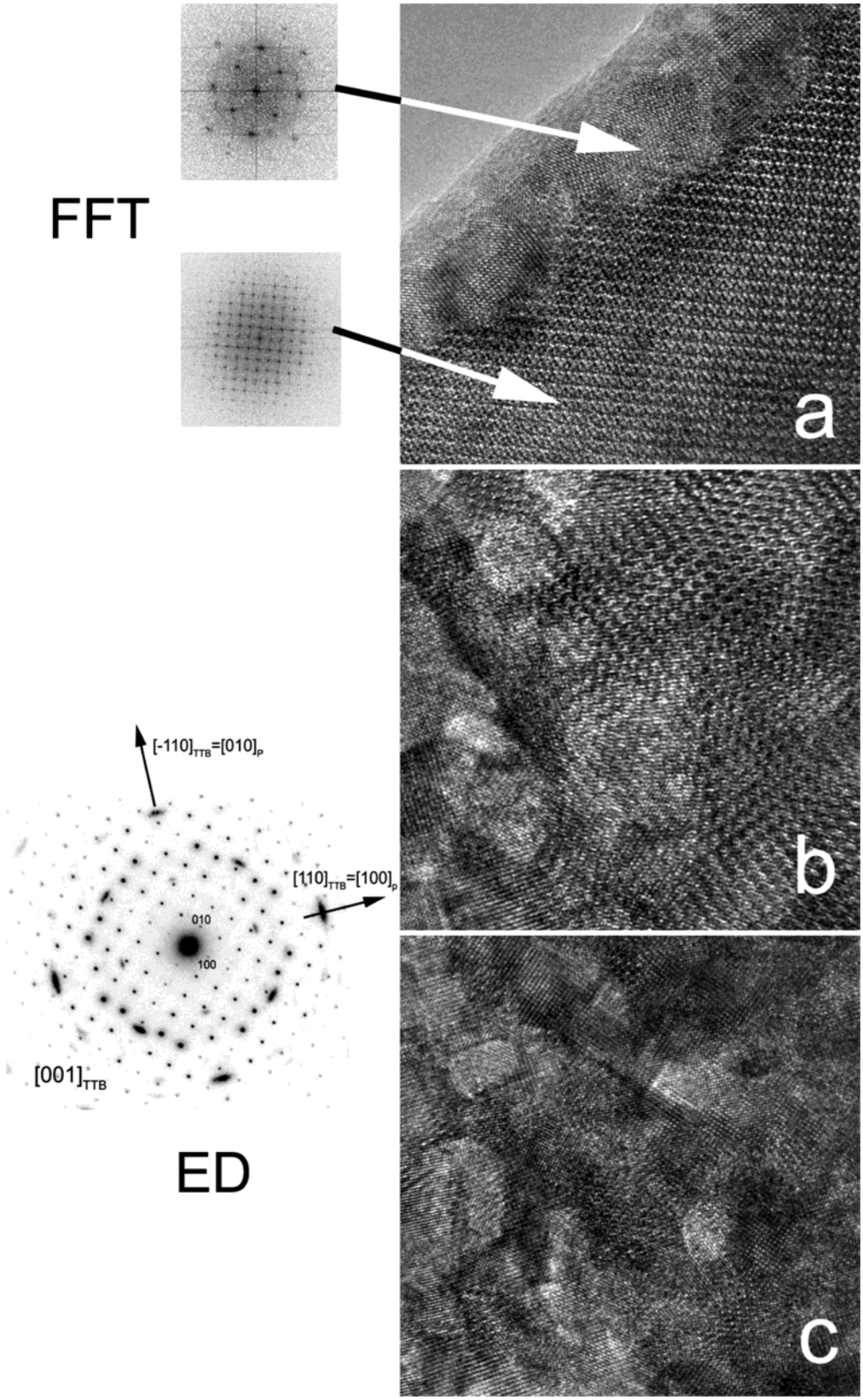

Figure 2. HREM images of a $K_{0.6}Mn^{II}_{0.6}Fe^{III}_{0.4}F_3$ sample showing the progressive decay of TTB structure to perovskite under the electron beam. (a) Initial growth of perovskite at the border of a bronze crystal, evidenced by Fourier transform of the image. (b) and (c) Images of the same area taken at successive times: the bronze structure (which occupies the right part of figure b) is gradually replaced by perovskite domains; the perovskite grows epitaxially, as evidenced in the corresponding ED pattern taken along the [001] zone axis.

Reaction products were identified by powder XRD analysis. Diffraction patterns were collected using Cu Kα radiation with a Thermo ARL X'tra powder diffractometer equipped with a Thermo Electron solid-state detector to eliminate the incoherent background produced by florescence in Fe- and Mn-containing samples. Data collection was performed by 0.01−0.02° steps with counting time ranging from 3 to 10 s. Single-crystal XRD data were collected on a Bruker AXS Smart

diffractometer, equipped with a CCD area detector and Mo Kα radiation.

Electron diffraction (ED) and high-resolution electron microscopy (HREM) were carried out using a Philips TECNAI F20 transmission electron microscope operating at 200 kV. The specimens were prepared by grinding the powder in isopropylic alcohol and evaporating the suspension on a copper grid covered with a holey carbon film.

Results and Discussion

Preliminary Characterization. The products of solid-state reactions were at first analyzed by powder XRD. For the composition $K_{0.4}M^{II}_{0.4}M^{III}_{0.6}F_3$, the products were found to consist of a single TTB phase, with the exception of the pure manganese compound for which the synthesis was unsuccessful. By increasing the K content to $x = 0.6$, the formation of KMF_3 perovskite becomes in some case competitive and the reaction results in a biphasic product, a major TTB phase with a K content lower than 0.6 and a minor perovskite impurity. The amount of perovskite depends critically on the choice of the M cations. Within the studied compositions, obviously not exhaustive of the different cationic combinations, single TTB phases were obtained for M = Fe or by partial substitution of Fe^{2+} by Mn^{2+}. The magnetic characterization of the samples obtained as single phase[22] showed generalized ferrimagnetic behavior, with T_N and magnetization strongly dependent on the composition and the nature of the M cations. The maximum in T_N and magnetization was found for Fe/Mn compounds in agreement with literature.[13] On the basis of powder XRD analysis all the synthesized compounds are tetragonal, with the exception of $K_{0.6}FeF_3$ which is orthorhombic.

TEM Characterization. The collection of ED patterns has been complicated by a generalized instability of TTB fluorides under the highly energized electron beam probing the sample; we directly observed by HREM images the gradual transition of TTB domains into perovskite structure. This returned a progressive degradation of the specimens and the appearance in ED patterns of diffraction spots characteristic of a perovskite phase superimposed over the bronze ones, together with concentric blur due to the presence of amorphous regions. ED analysis evidenced that perovskite grows epitaxially over TTB domains, sharing [100] with $[110]_{TTB}$ directions (Figure 2). According to our preparative results, showing a major competition of perovskite with TTB formation for $x = 0.6$, the faster decomposition kinetics was observed for these samples.

ED analysis performed at room temperature showed a strong analogy of the fluoride bronzes with the orthorhombic phase of $Ba_2NaNb_5O_{15}$ (BNN). In particular, modulation satellites, similar to those characteristic of the room-temperature BNN phase, were observed for every examined sample. At high temperature BNN is tetragonal, space group *P*4/*mbm*, and paraelectric. At 853 K it undergoes a standard ferroelectric transition ($4/mmm \rightarrow 4mm$) that is accompanied by a divergence of the dielectric susceptibility along the *c* axis.[23] The symmetry decrease to *P*4*bm* involved in the phase transition is mainly determined by the displacement of the niobium atoms from the basal plane of its octahedral oxygen coordination, which results in a remarkable difference in the two apical distances. Below 573 K the symmetry decreases to *mm2* and the orthorhombic

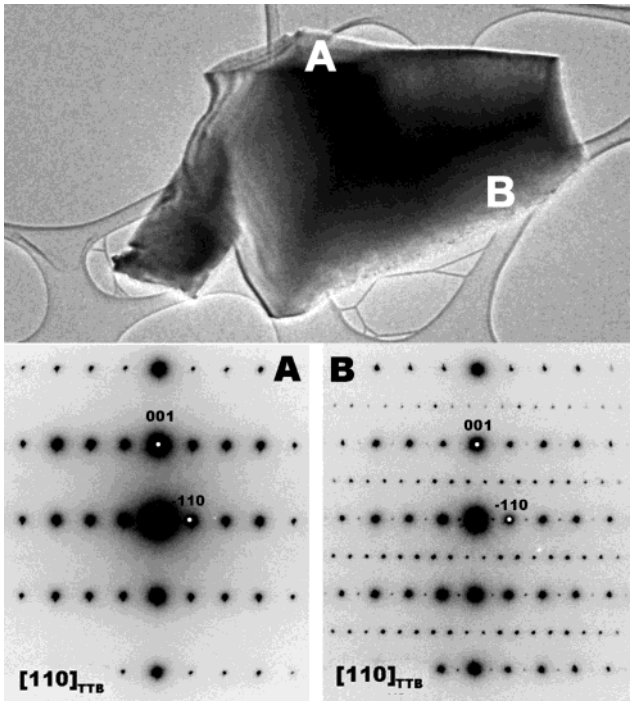

Figure 3. SAED patterns taken in the same TTB zone axis on two different regions (marked as A and B) of a single grain $K_{0.4}Fe_{0.8}In_{0.2}F_3$ sample: the patterns are consistent with the twinning domains expected for the FES structure (see text for details).

region is characterized by the existence of a quasi-commensurate modulation along the $[110]_{TTB}$ direction, connected to the doubling of the *c* parameter (~8 Å). The symmetry decrease from tetragonal to orthorhombic is ascribed to the existence of a cooperative tilting of the $[NbO_6]$ octahedra. The fundamental averaged structure at room temperature was determined at the end of the 1960s by Jamieson et al.[24] The first attempt to describe the modulated structure was made by Lin and Bursill[25] on the basis of ED data in an orthorhombic supercell with $a \approx b \approx 2\ a_{TTB}\sqrt{2}$, $c = 2\ c_{TTB}$ and space group *Im*2*a*. Further studies on de-twninned crystals by Labbé et al.[26] demonstrated that the supercell describing the quasi-commensurate modulation is in reality half in volume, being $b \approx a_{TTB}\sqrt{2}$, and its symmetry is consistent with the *Bbm*2 space group. The use of de-twninned crystals revealed to be fundamental in structural studies of BNN. In fact, the unavoidable occurrence of phase transitions during the room-temperature cooling of tetragonal BNN crystals grown at high temperature, typically results in a severe twinning consisting of four orientation variants. They correspond to two possible orientations of the polar *c* axis and to two possible orientations of the orthorhombic *a* axis. The former give rise to ferroelectric domains tilted by 180°, whereas the latter give rise to ferroelastic domains. Both can be detected by transmission electron microscopy

(22) Fabbrici, S. Laurea Thesis, Parma University, 2003.
(23) Shing, S.; Draggert, D. A.; Geusic, J. E. *Phys Rev*. **1970**, B *2*, 2709.
(24) Jamieson, P. B.; Abrahams S. C.; Bernstein, J. L. *J. Chem. Phys*. **1969**, *50*, 4352.
(25) Ju Lin, P.; Bursill, L. A. *Acta Crystallogr., Sect. B: Struct. Sci.* **1987**, *43*, 504.
(26) Labbé, P.; Leligny, H.; Raveau, B.; Scheck, J.; Toledano, J. C. *J. Phys. Condens. Matter* **1989**, *2*, 25.

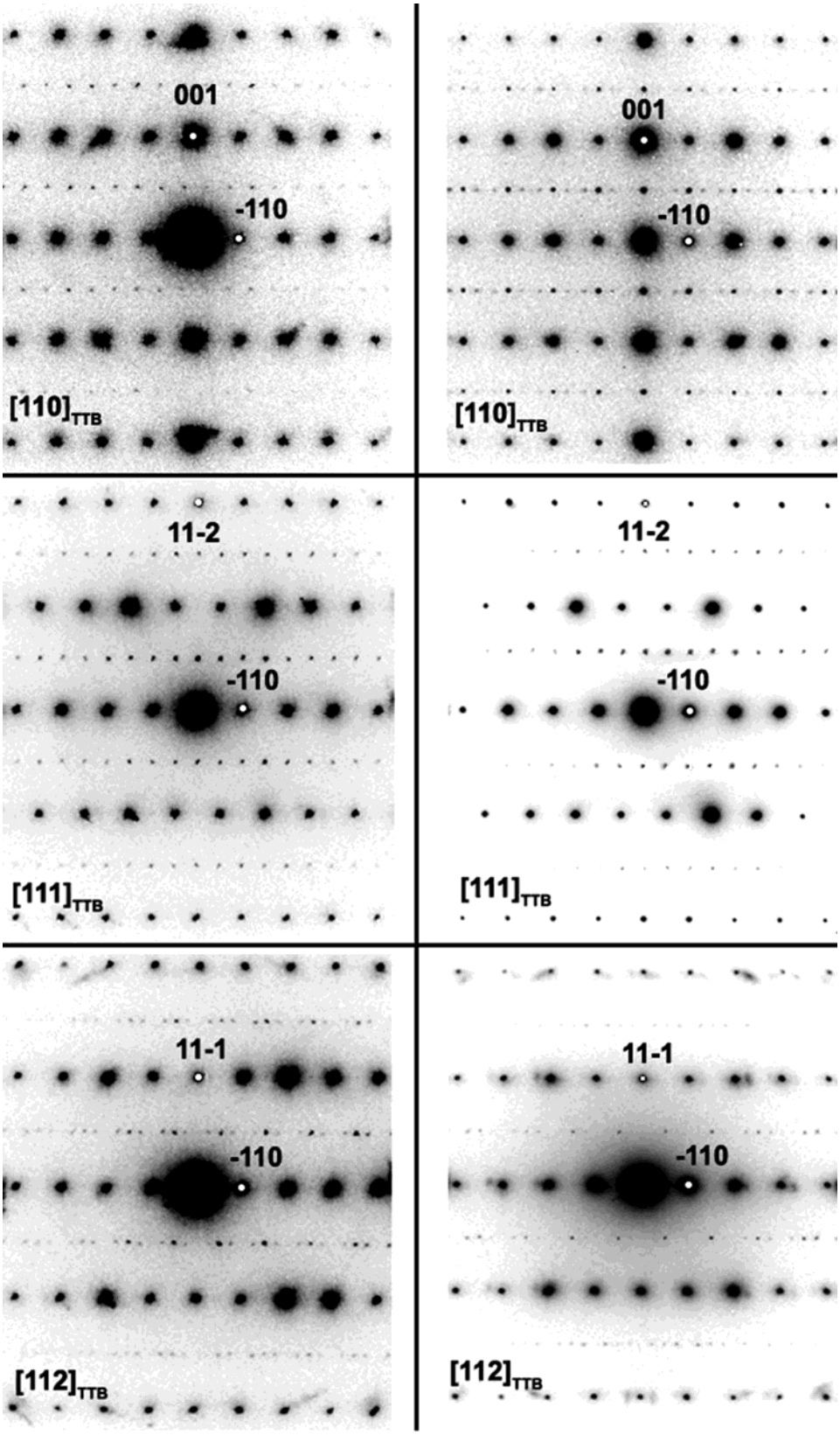

Figure 4. ED patterns along different zone axes for crystals of composition $K_{0.4}MF_3$ (on the left) and of composition $K_{0.6}MF_3$ (on the right). Fundamental spots are indexed on the basis of the TTB cell.

(TEM) by using diffraction contrast techniques. The removal of twinning domains requires reheating above the ferroelectric transition followed by cooling under compressive stress and electric field. In the absence of de-twinning processes, the observation of the double supercell found by Lin and Bursill[25] is quite typical in BNN, because the ferroelastic twinning occurs at a range so short that even in selected area ED (SAED), results show the illuminated region (few hundreds of square nm) to consist of different domains.

A similar twinning occurs also in TTB fluorides, but fortunately the domains are much more extended than

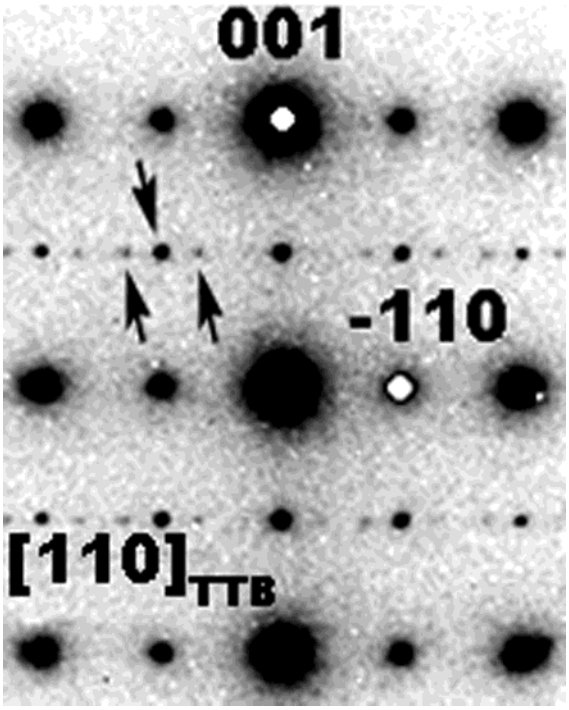

Figure 5. Two classes of modulation satellites typically observed in ED patterns of TTB fluorides; upward arrows point at FES modulation satellites, downward arrow points at COS modulation satellites. The example in the figure refers to the compound $K_{0.6}Mn^{II}_{0.6}Fe^{III}_{0.4}F_3$

those in BNN so SAED is able to characterize single domains. Figure 3 shows a low magnification image of single grain $K_{0.4}Fe_{0.8}In_{0.2}F_3$ and the corresponding $[110]_{TTB}$ SAED patterns obtained from two different regions marked as A and B. The patterns share the same fundamental spots, typical of the TTB structure, but differ in the presence of modulation satellites which appear in the B pattern; the satellites are the same appearing in the room-temperature quasi-commensurate phase of BNN, and could be indexed on the basis of the TTB cell only through semi-integer indices (n/2 and n/4). By taking into account the supercell introduced by Labbé et al.[26] for BNN, thereinafter indicated as ferroelastic superstructure (FES), the A and B diffraction patterns match with zone axis $[010]_{FES}$ and $[100]_{FES}$, respectively. In this hypothesis A and B would represent two distinct domains turned 90° around the *c* axis.

A systematic study of the reciprocal lattice, carried out by a series of SAED in different zone axis and for different compositions, always showed the presence of modulation satellites which are fully compatible with the periodicity and symmetry of the FES structure. A typical example is shown in Figure 4, where some corresponding patterns of Fe and Fe−Mn based compounds are compared. This allows the conclusion, at least on a qualitative basis, that at room temperature the TTB fluorides share with niobates a peculiar structural modulation, related to cooperative tilt of $[MF_6]$ octahedra, which represents in the latter the typical signature of ferroelasticity.

Differently from BNN, ED revealed in our samples (Figure 5) the presence of an additional set of commensurate modulation spots which could be still indexed with the FES periodicity, but on one side they violate the extinction rules of the FES symmetry and on the other side, unlike typical FES modulation spots, they are composition dependent. If the FES satellites are neglected, the indexing of these additional spots requires simply the doubling of the c_{TTB} axis, giving rise to the supercell that has been previously utilized in the literature to describe the structure of $K_{0.54}(Mn,Fe)F_3$ and $K_{0.38}Mg_{0.38}In_{0.62}F_3$. Since the modulation symmetry depends on the composition and the spot intensities are dependent on the nature of the divalent and trivalent cations, the origin of this modulation was from the beginning attributed to the presence of charge order and the related cell is thereinafter indicated as charge order superlattice (COS).

The symmetry of COS modulation is related to the M^{II}/M^{III} ratio, and consequently to the K content. In case of $K_{0.4}MF_3$ compounds, the systematic extinctions observed for $h0l$ with $h = 2n + 1$, $0kl$ with $k = 2n + 1$, and hhl with $l = 2n + 1$ (which are consistent with the presence of two pairs of mutually orthogonal glides tilted by 45°) limits the choice to the tetragonal space groups $P4_2bc$ or $P4_2/mbc$, where the first has to be considered in case of ferroelectricity of the system. This result is consistent with the structural determination previously reported Banks et al.[8] for $K_{0.54}(Mn,Fe)F_3$. On the contrary, when $K_{0.6}MF_3$ compounds are concerned, the condition hhl, $l = 2n$ limiting the possible reflections disappears; considering only noncentrosymmetric space groups we get two possible solutions: tetragonal *P4bm* or orthorhombic *Pba*2. Whereas for the $K_{0.6}Fe^{II}_{0.6}Fe^{III}_{0.4}F_3$ iron-based fluoride powder XRD analysis clearly pointed out the orthorhombic distortion of the TTB structure (for which *Pba*2 represents a suitable description), no appreciable distortion was found in the case of $K_{0.6}MF_3$ compounds where iron is partially substituted by a different cation. It must be noticed that the space group *Pba*2 has been reported in the literature for the $K_{0.6}Fe^{II}_{0.6}Fe^{III}_{0.4}F_3$ structure, but referred to a conventional TTB cell and not to the double cell clearly indicated by our ED patterns. On the other hand *P4bm* is the typical space group observed for ferroelectric tetragonal TTB niobates, but also in this case referred to the conventional TTB cell, whose extension along the *c* axis ($c_{TTB} \approx 4$ Å) is limited to the thickness of a single layer of $[NbO_6]$ octahedra. Since both the space groups have equivalent positions at the same height *z*, the two octahedral layers forming the COS cell (generated by different equivalent positions in both the space groups) must differ in some extent to justify the appearing of satellite reflections related to the doubling of the *c* axis.

Single-Crystal XRD. The crystal structure of $K_{0.525}Fe^{II}_{0.525}Fe^{III}_{0.475}F_3$ was analyzed on the basis of single-crystal XRD by using the information obtained a priori by ED experiments. Some crystals obtained in the same batch were preliminarily tested by using a Bruker SMART system equipped with a CCD area detector. The presence of both FES and COS satellites was detected for all the examined samples, and a crystal showing single-domain FES characteristics was selected for the data collection on the same diffractometer. Three different data reductions were performed on the basis of conventional TTB, COS, and FES cells, respectively. We approached the structural solution by steps: the mean TTB structure was refined at first by considering only the fundamental reflections; the averaged informa-

Table 1. Crystallographic Data and Refining Parameters for $K_{0.525}FeF_3$

empirical formula	$K_{0.525}Fe\ F_3$
fw	133.37 g/mol
temp	293(2) K
wavelength	0.71069 Å
density (calcd)	3.51 g/cm^3
abs coeff	6.65 mm^{-1}
cryst size	0.064 × 0.048 × 0.113 mm^3
refinement method	full-matrix least-squares on F^2

Identification code	TTB	FES	COS
cryst syst	tetragonal	orthorhombic	tetragonal
space group	*P*4*bm*	*Bbm*2	$P4_2bc$
unit cell dimensions	a = 12.634(1) Å	a = 35.730(3) Å	a = 12.634(1) Å
	b = 12.634(1) Å	b = 17.872(1) Å	b = 12.634(1) Å
	c = 3.9515(3) Å	c = 7.9030(6) Å	c = 7.9030(6) Å
vol	630.73(9) Å^3	5046.6(7) Å^3	1261.5(2) Å^3
Z	10	80	20
θ range (data collection)	2.28 to 27.50°	1.61 to 27.49°	2.28 to 27.48°.
index ranges			
h	−15 to 15	−44 to 46	−14 to 16
k	−15 to 15	−15 to 22	−15 to 15
l	−5 to 5	−9 to 10	−9 to 10
reflns collected	5162	14349	6625
independent reflns	753 [R_{int} = 0.0373]	5333 [R_{int} = 0.0259]	1395 [R_{int} = 0.0449]
data/restraints/params	747/1/63	4281/1/445	1272/1/110
GOF on F^2	1.000	0.746	0.978
R indices [$I > 2\sigma(I)$]	R1 = 0.0215	R1 = 0.0225	R1 = 0.0209,
	wR2 = 0.0497	wR2 = 0.0506	wR2 = 0.0544
R indices (all data)	R1 = 0.0272	R1 = 0.0939	R1 = 0.0402
	wR2 = 0.0515	wR2 = 0.0758	wR2 = 0.0613
largest diff. peak and hole	0.477 and −0.457 eÅ^{-3}	0.622 and −0.578 eÅ^{-3}	0.519 and −0.335 eÅ^{-3}

Table 2. Refined Atomic Coordinates (× 10^4) and Thermal Parameters (Å^2 × 10^3) of the TTB Structure

atom	x	y	z	U(eq)	U_{11}	U_{22}	U_{33}	U_{23}	U_{13}	U_{12}
Fe(1)	1/2	0	4988(10)	12(1)	11(1)	11(1)	13(1)	0	0	0(1)
Fe(2)	2120(1)	742(1)	1/2	12(1)	13(1)	11(1)	12(1)	−1(1)	0(2)	0(1)
K(1)	1723(1)	3277(1)	−7(18)	41(1)	51(1)	51(1)	22(1)	−2(2)	2(2)	26(1)
K(2)[a]	0	0	36(29)	17(1)	17(1)	17(1)	18(1)	0	0	0
F(1)	1432(1)	−702(1)	4883(29)	34(1)	33(1)	19(1)	50(1)	4(4)	−8(5)	−4(1)
F(2)	2808(1)	2192(1)	4942(39)	25(1)	22(1)	22(1)	32(2)	2(4)	−2(4)	−2(1)
F(3)	3456(1)	−67(2)	4887(27)	38(1)	15(1)	38(1)	61(2)	−16(4)	−4(4)	2(1)
F(4)	1/2	0	−175(73)	52(1)	71(2)	71(2)	15(3)	0	0	−3(2)
F(5)	2090(2)	766(2)	−165(44)	42(1)	43(1)	75(2)	9(2)	2(4)	−3(4)	−20(1)

[a] Site occupancy factor 0.625(4).

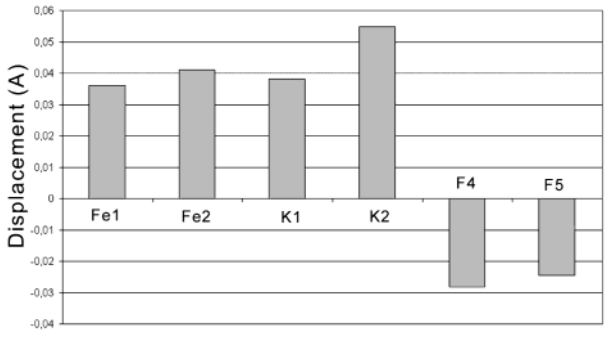

Figure 6. Relative displacements of cations and apical fluorine atoms with respect to the mean plane defined by the basal fluorine atoms.

tion was then used for refining both FES and COS structures, by considering in first approximation the two modulations as mutually independent; the refinements confirmed the starting hypothesis on the origin of the modulations and led to the definition of the real structure.

(a) TTB Refining. By taking into account only the fundamental reflections the cell was found to be tetragonal, with systematic extinctions compatible with *P*4/*mbm* or *P*4*bm* space groups. Since the literature

Table 3. Interatomic Distances [Å] in the TTB Structure

Fe(1)−F(3)	1.953(2)	Fe(2)−F(5)	1.911(17)
Fe(1)−F(3)	1.953(2)	Fe(2)−F(3)	1.974(2)
Fe(1)−F(3)	1.953(2)	Fe(2)−F(1)	1.993(2)
Fe(1)−F(3)	1.953(2)	Fe(2)−F(1)	2.021(2)
Fe(1)−F(4)	1.911(28)	Fe(2)−F(2)	2.028(1)
Fe(1)−F(4)	2.040(28)	Fe(2)−F(5)	2.042(17)
average	1.960(2)	average	1.9943(4)

associates the ferroelectricity in the K_xFeF_3 system with the orthorhombic distortion that occurs at higher x values, the refinement has been initially carried out with SHELX93[27] in both space groups. The refinement supplied a sure indication of the noncentrosymmetric space group as the most suitable for the structure description. The crystal under examination was found to be affected by ferroelectric polar twinning, and the contributions of the two twinning domains were refined and found to be almost equivalent. Crystallographic data and refinement parameters for *P*4*bm* are reported in Table 1; atomic parameters are reported in Table 2. The refined occupancy factors of potassium ions returned a crystal composition $K_{0.525}Fe^{II}_{0.525}Fe^{III}_{0.475}F_3$: the A_2 site was found to be completely filled, while the

(27) Sheldrick, G. M. *SHELXL93, Program for Crystal Structure Refinement*; University of Gottingen, Germany, 1993.

Table 4. Refined Atomic Coordinates (× 10^4) and Thermal Parameters (Å^2 × 10^3) of the FES Structure

atom	*x*	*y*	*z*	*U*(eq)	U_{11}	U_{22}	U_{33}	U_{23}	U_{13}	U_{12}
Fe(1)	4283(1)	690(1)	2917(3)	13(1)	15(1)	10(1)	14(1)	1(1)	3(1)	4(1)
Fe(2)	1783(1)	−687(1)	2920(3)	12(1)	14(1)	10(1)	13(1)	1(1)	−1(1)	3(1)
Fe(3)	3215(1)	687(1)	2924(3)	11(1)	15(1)	7(1)	11(1)	0(1)	1(1)	0(1)
Fe(4)	714(1)	−690(1)	2918(3)	11(1)	9(1)	11(1)	13(1)	−1(1)	−2(1)	−3(1)
Fe(5)	2155(1)	1429(1)	2904(2)	10(1)	12(1)	9(1)	8(1)	2(1)	0(1)	−2(1)
Fe(6)	346(1)	1434(1)	2927(2)	13(1)	17(1)	9(1)	15(1)	−2(1)	0(1)	1(1)
Fe(7)	4655(1)	−1431(1)	2912(2)	12(1)	14(1)	8(1)	14(1)	2(1)	0(1)	−1(1)
Fe(8)	2843(1)	−1429(1)	2916(2)	12(1)	9(1)	14(1)	14(1)	−3(1)	−1(1)	−1(1)
Fe(9)	1247(1)	3/4	2919(4)	11(1)	15(1)	6(1)	14(1)	0	4(1)	0
Fe(10)	3750(1)	1/4	2916(4)	12(1)	11(1)	13(1)	13(1)	0	−3(1)	0
Fe(11)	3748(1)	3/4	2931(4)	11(1)	14(1)	6(1)	14(1)	0	0(1)	0
Fe(12)	1253(1)	1/4	2926(4)	12(1)	11(1)	13(1)	13(1)	0	0(1)	0
K(1)[a]	0	0	410(12)	13(1)	14(2)	19(3)	7(2)	0	0	3(2)
K(2)[b]	1/2	0	412(13)	12(1)	9(2)	18(3)	10(3)	0	0	0(2)
K(3)	2876(1)	1/4	388(9)	34(1)	21(1)	57(2)	24(2)	0	3(3)	0
K(4)	2901(1)	1/4	5406(10)	44(1)	18(1)	88(3)	26(2)	0	−4(3)	0
K(5)	5387(1)	3/4	5394(10)	40(1)	31(2)	69(2)	18(2)	0	−1(3)	0
K(6)	−385(1)	1/4	5417(10)	42(1)	32(2)	71(2)	22(2)	0	5(3)	0
K(7)[c]	2500(1)	1(1)	414(11)	22(1)	23(2)	11(2)	32(3)	−3(2)	−8(2)	1(1)
K(8)	3776(1)	−769(1)	5407(7)	38(1)	66(1)	23(1)	24(1)	0(2)	2(3)	−13(1)
K(9)	1284(1)	794(1)	5408(7)	39(1)	74(1)	22(1)	22(1)	−2(2)	−4(3)	−3(1)
F(1)	148(3)	1/4	2775(17)	30(3)	29(6)	31(7)	30(8)	0	−4(6)	0
F(2)	2360(3)	1/4	2984(16)	27(3)	23(6)	46(7)	12(5)	0	−2(5)	0
F(3)	2665(3)	3/4	2758(16)	21(3)	12(5)	9(5)	43(8)	0	−2(5)	0
F(4)	4835(3)	3/4	2977(16)	17(2)	24(5)	1(4)	27(6)	0	−4(6)	0
F(5)	1970(2)	361(4)	2733(12)	32(2)	31(4)	20(4)	44(6)	2(4)	6(4)	−19(3)
F(6)	534(2)	360(5)	3024(13)	34(2)	42(5)	27(5)	32(5)	−6(5)	−2(5)	7(4)
F(7)	2677(2)	1061(4)	2969(12)	26(2)	22(4)	18(4)	38(5)	3(4)	4(4)	2(3)
F(8)	4460(2)	−369(4)	2739(12)	27(2)	19(4)	10(4)	52(6)	4(4)	1(5)	12(3)
F(9)	4809(2)	1074(5)	3041(12)	30(2)	31(4)	38(5)	23(4)	−1(5)	1(5)	2(4)
F(10)	188(2)	−1065(5)	2729(12)	29(2)	6(3)	31(5)	50(6)	6(5)	−1(4)	−11(3)
F(11)	3023(2)	−366(4)	2960(12)	30(2)	35(4)	23(5)	33(5)	−7(4)	2(4)	9(3)
F(12)	2327(2)	−1075(5)	2709(12)	34(2)	30(4)	24(5)	47(7)	−1(4)	−2(4)	18(3)
F(13)	1254(2)	−301(3)	2979(13)	23(2)	37(4)	16(3)	18(3)	−2(4)	−5(4)	3(4)
F(14)	3752(2)	313(4)	2791(12)	24(2)	12(3)	26(4)	34(5)	−6(4)	2(4)	−7(4)
F(15)	891(2)	1664(5)	3076(12)	31(2)	32(4)	32(4)	29(4)	20(4)	−13(4)	−21(3)
F(16)	3382(2)	−1712(5)	3099(13)	31(2)	29(4)	28(4)	36(5)	1(5)	−6(5)	5(3)
F(17)	1624(2)	1697(5)	2728(13)	31(2)	20(4)	27(5)	47(6)	0(5)	1(5)	17(4)
F(18)	4119(2)	−1695(4)	2698(12)	32(2)	24(4)	12(4)	61(7)	−1(4)	−2(5)	1(3)
F(19)	4158(2)	1771(4)	3005(11)	24(2)	33(4)	12(4)	26(4)	1(4)	−15(4)	13(3)
F(20)	1658(2)	−1760(5)	3000(14)	39(2)	29(5)	40(5)	46(6)	11(5)	−1(5)	−2(4)
F(21)	3348(2)	1750(4)	2707(13)	32(2)	22(4)	17(4)	56(6)	−2(4)	−6(5)	−7(3)
F(22)	855(2)	−1759(5)	2721(12)	38(3)	34(4)	13(4)	66(7)	−13(5)	4(5)	16(3)
F(23)	4722(1)	−1479(2)	387(14)	26(1)	42(3)	26(3)	8(3)	−8(5)	−2(5)	6(2)
F(24)	2218(1)	1453(3)	350(15)	32(1)	52(3)	30(3)	12(3)	−1(5)	4(6)	14(2)
F(25)	3191(1)	612(3)	373(15)	32(1)	33(3)	58(3)	5(3)	−7(5)	−4(5)	−14(2)
F(26)	4310(1)	774(3)	372(15)	32(1)	38(3)	38(3)	20(3)	18(5)	−1(5)	8(2)
F(27)	3795(2)	1/4	374(22)	43(2)	51(4)	55(4)	21(3)	0	19(8)	0
F(28)	1201(2)	1/4	320(22)	45(2)	77(5)	46(3)	11(3)	0	1(8)	0
F(29)	3248(1)	697(3)	5347(15)	37(2)	40(3)	68(4)	4(3)	−14(5)	−6(5)	−2(2)
F(30)	4270(1)	576(3)	5341(15)	28(1)	26(2)	37(3)	22(3)	−13(5)	−5(5)	4(2)
F(31)	2115(1)	1375(2)	5369(14)	29(1)	48(3)	23(3)	15(3)	−8(5)	−13(5)	3(2)
F(32)	4615(1)	−1395(3)	5307(16)	35(2)	55(3)	38(3)	11(3)	−7(5)	3(5)	−10(2)
F(33)	3692(2)	1/4	5429(21)	34(2)	39(4)	51(3)	13(3)	0	−10(8)	0
F(34)	1320(1)	1/4	5378(19)	27(1)	12(3)	46(3)	21(3)	0	15(7)	0

[a] Site occupancy factor 0.580(7). [b] Site occupancy factor 0.569(7). [c] Site occupancy factor 0.669(6).

A_1 site (perovskite-like site) occupancy level was found to be limited to 62%.

Clearly, the structure obtained by this refinement supplies the mean situation projected onto the fundamental cell, but it contains valuable information. The refinement suggests the presence of static disorder. Anisotropic displacement parameters of fluorine atoms are rather high: apical atoms possess high values in the *xy* plane, while basal ones show thermal motion elongated along the *z* axis. This could be easily interpreted as superposition of different sites originated from tilting of [FeF_6] octahedra. Similar anisotropic displacement parameter anomalies could be seen for the K(2) site, as its position should be influenced from the propagation of the tilt wave. Despite this, the averaged atomic positions of the TTB structure give information on the ferroelectric distortion (Figure 6). All the cations lie, along the *c* axis, above the mean plane of basal fluorine anions, whereas the apical fluorine atoms are displaced in the opposite direction. The displacement direction of the cations is chosen as the positive of the polar axis. Refined bond distances are reported in Table 3. The two Fe−F apical distances for each Fe atom are different, the shorter pointing toward the positive direction of the polar axis. The average Fe−F distance is significantly shorter for Fe(1) (1.960(2) Å), indicating an occupational preference of divalent Fe on the perovskite-like site Fe(2) (1.9943(2) Å).

(b) FES Refining. Structure solution and refinement was achieved considering both fundamental reflections

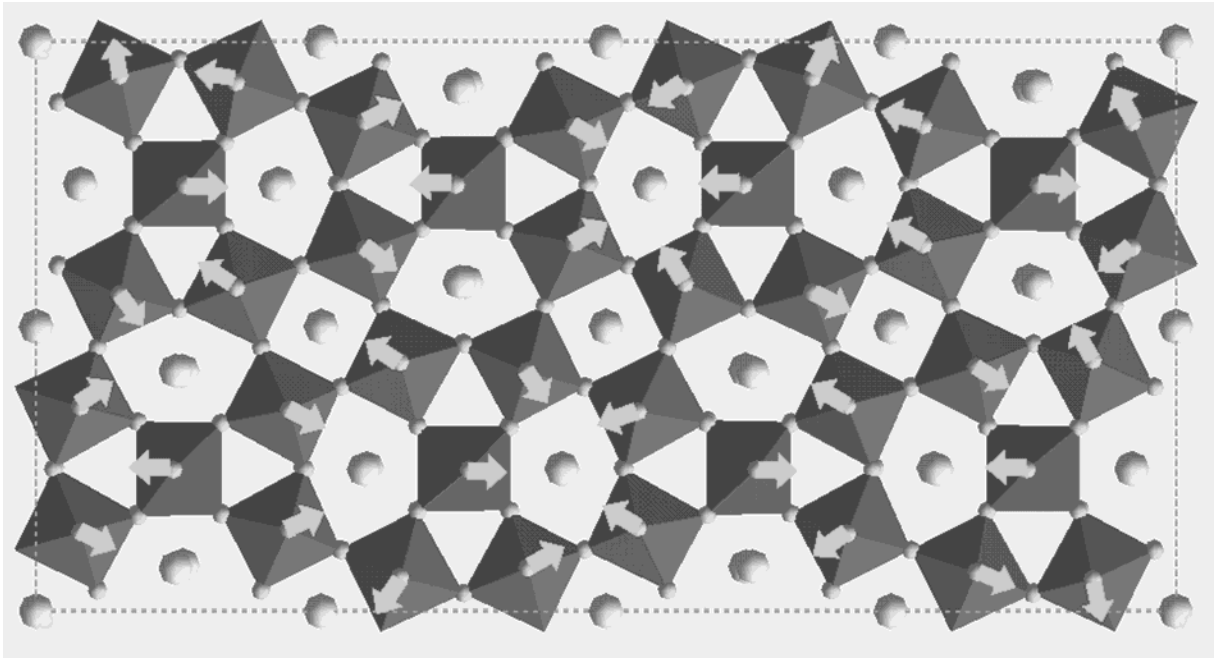

Figure 7. View, along the *c* axis, of the orthorhombic FES supercell; tilting directions of the apical fluorine atoms are evidenced for clarity.

Table 5. Interatomic Distances [Å] in the FES Structure

Fe(1)−F(19)	1.984(8)	Fe(5)−F(17)	1.963(8)	Fe(9)−F(22)	1.933(8)
Fe(1)−F(9)	2.003(8)	Fe(5)−F(7)	1.976(8)	Fe(9)−F(22)	1.933(8)
Fe(1)−F(8)	2.000(7)	Fe(5)−F(5)	2.024(7)	Fe(9)−F(20)	1.976(9)
Fe(1)−F(14)	2.015(7)	Fe(5)−F(2)	2.051(4)	Fe(9)−F(20)	1.976(9)
Fe(1)−F(30)	1.926(12)	Fe(5)−F(31)	1.955(11)	Fe(9)−F(27)	1.946(17)
Fe(1)−F(26)	2.020(12)	Fe(5)−F(24)	2.031(12)	Fe(9)−F(33)	1.980(16)
average	1.991(4)	average	2.000(4)	average	1.958(5)
Fe(2)−F(20)	1.970(9)	Fe(6)−F(15)	1.995(8)	Fe(10)−F(19)	1.957(8)
Fe(2)−F(5)	1.994(7)	Fe(6)−F(10)	2.022(7)	Fe(10)−F(19)	1.957(7)
Fe(2)−F(13)	2.013(8)	Fe(6)−F(1)	2.037(5)	Fe(10)−F(21)	1.970(8)
Fe(2)−F(12)	2.068(8)	Fe(6)−F(6)	2.035(8)	Fe(10)−F(21)	1.970(8)
Fe(2)−F(25)	1.946(12)	Fe(6)−F(23)	1.961(11)	Fe(10)−F(33)	1.997(16)
Fe(2)−F(29)	2.037(11)	Fe(6)−F(32)	2.077(12)	Fe(10)−F(27)	2.016(17)
average	2.005(4)	average	2.021(4)	average	1.979(5)
Fe(3)−F(21)	1.966(8)	Fe(7)−F(18)	1.979(8)	Fe(11)−F(16)	1.924(8)
Fe(3)−F(11)	2.004(8)	Fe(7)−F(4)	2.016(4)	Fe(11)−F(16)	1.924(8)
Fe(3)−F(14)	2.036(8)	Fe(7)−F(8)	2.027(7)	Fe(11)−F(18)	1.966(9)
Fe(3)−F(7)	2.036(7)	Fe(7)−F(9)	2.022(8)	Fe(11)−F(18)	1.966(8)
Fe(3)−F(29)	1.918(11)	Fe(7)−F(32)	1.899(12)	Fe(11)−F(28)	1.897(17)
Fe(3)−F(25)	2.022(12)	Fe(7)−F(23)	2.012(11)	Fe(11)−F(34)	2.032(14)
average	1.997(4)	average	1.993(4)	average	1.952(5)
Fe(4)−F(6)	1.985(8)	Fe(8)−F(12)	1.957(8)	Fe(12)−F(17)	1.960(8)
Fe(4)−F(22)	1.983(8)	Fe(8)−F(16)	1.998(8)	Fe(12)−F(17)	1.960(8)
Fe(4)−F(10)	2.003(7)	Fe(8)−F(11)	2.007(8)	Fe(12)−F(15)	1.979(8)
Fe(4)−F(13)	2.053(9)	Fe(8)−F(3)	2.020(4)	Fe(12)−F(15)	1.979(8)
Fe(4)−F(26)	1.947(12)	Fe(8)−F(24)	1.937(12)	Fe(12)−F(34)	1.953(15)
Fe(4)−F(30)	2.048(12)	Fe(8)−F(31)	2.021(11)	Fe(12)−F(28)	2.068(17)
average	2.003(4)	average	1.990(4)	average	1.983(5)

and modulation satellites typical of the BNN structure. The FES cell is orthorhombic, space group *Bbm*2, with $a = 2a_{TTB}\sqrt{2}$, $b = a_{TTB}\sqrt{2}$, and $c = 2c_{TTB}$. The *c* axis is doubled, so that the cell volume becomes 8 times the TTB one. Differently from BNN and related systems, the modulation is commensurate in these fluorides. The structure has been solved ab initio in the FES cell with SIR2002,[28] and the full matrix was refined with SHELX93.[27] Crystallographic data and refinement parameters are reported in Table 1, and refined atomic parameters are shown in Table 4. A projection of the structure along the *c* axis is shown in Figure 7.

Structural results evidence the presence of a tilt modulation: [FeF_6] octahedra are tilted with respect to the *c* axis and the tilt propagates cooperatively in the *ab* plane by the corner sharing of the octahedra. Tilt propagation and values of atomic displacement are similar to those obtained in the corresponding BNN structure.[26] This on one side represents an indirect confirmation of the results of Labbé et al. and at the same time proves that the tilt modulation, related to the appearance of ferroelasticity in BNN, is not a unique

(28) Altomare, A.; Burla, M. C.; Camalli, M.; Cascarano, G.; Giacovazzo, C.; Guagliardi, A.; Moliterni, A. G. G.; Polidori, G.; Spagna, R. *SIR2002, Program for Crystal Structure Solution and Refinement*; IRMEC-CNR, Bari, Italy, 2002.

Table 6. Refined Atomic Coordinates (× 10^4) and Thermal Parameters (Å^2 × 10^3) of the COS Structure

atom	*x*	*y*	*z*	*U*(eq)	U_{11}	U_{22}	U_{33}	U_{23}	U_{13}	U_{12}
Fe(1)	1/2	0	2104(4)	12(1)	12(1)	10(1)	13(1)	0	0	0(1)
Fe(2)	2131(1)	−742(1)	7105(2)	12(1)	12(1)	11(1)	12(1)	1(1)	0(1)	−1(1)
Fe(3)	2110(1)	−742(1)	2096(2)	12(1)	12(1)	10(1)	13(1)	1(1)	1(1)	0(1)
K(1)	1719(2)	−3273(2)	4597(8)	42(1)	52(2)	51(2)	24(1)	3(2)	0(2)	−26(1)
K(2)[a]	0	0	−394(12)	18(1)	19(3)	14(3)	20(1)	0	0	4(3)
F(1)	2759(1)	−2143(1)	2055(15)	23(1)	21(1)	16(1)	33(1)	−2(4)	−5(4)	5(1)
F(2)	3442(1)	−11(2)	2036(15)	41(1)	16(1)	28(1)	77(3)	13(6)	3(5)	−5(1)
F(3)	5146(2)	−1531(1)	2101(15)	29(1)	23(1)	13(1)	53(2)	2(5)	−2(6)	−4(1)
F(4)	1490(2)	672(2)	2052(13)	33(1)	29(1)	17(1)	53(2)	−3(4)	−9(5)	5(1)
F(5)	732(2)	−1373(1)	2049(13)	31(1)	16(1)	26(1)	51(2)	3(5)	−2(4)	−8(1)
F(6)	2077(5)	−747(5)	4482(15)	44(2)	35(4)	82(6)	14(4)	−2(4)	0(3)	21(3)
F(7)	2102(5)	−783(5)	−394(16)	42(2)	51(5)	70(5)	6(3)	6(4)	1(4)	24(3)
F(8)	1/2	0	4573(27)	53(1)	65(8)	74(9)	18(2)	0	0	6(2)

[a] Site occupancy factor 0.627(3).

Table 7. Interatomic Distances [Å] in the COS Structure

Fe(1)−F(3)	1.942(2)	Fe(2)−F(3)	2.030(2)	Fe(3)−F(5)	1.915(2)
Fe(1)−F(3)	1.942(2)	Fe(2)−F(4)	2.072(2)	Fe(3)−F(2)	1.921(2)
Fe(1)−F(2)	1.969(2)	Fe(2)−F(5)	2.094(2)	Fe(3)−F(1)	1.951(2)
Fe(1)−F(2)	1.969(2)	Fe(2)−F(1)	2.105(2)	Fe(3)−F(4)	1.951(2)
Fe(1)−F(8)	1.952(22)	Fe(2)−F(7)	1.978(14)	Fe(3)−F(6)	1.886(14)
Fe(1)−F(8)	2.000(22)	Fe(2)−F(6)	2.075(13)	Fe(3)−F(7)	1.968(14)
average	1.962(5)	average	2.059(4)	average	1.932(4)

Table 8. Charge Distribution Calculation Results Carried out with CHARDIS[26] from Structural Data Provided from the COS Refinement[a]

cation	*q*(ij)	*Q*(ij)	ECoN	*q*(ij)/*Q*(ij)	anion	*q*(k)	*Q*(k)	*q*(k)/*Q*(k)
Fe(1)	2.38	2.386	5.653	0.998	F(1)	−1.00	−1.018	0.983
Fe(2)	2.00	2.015	4.807	0.992	F(2)	−1.00	−1.087	0.920
Fe(3)	3.00	2.987	5.216	1.004	F(3)	−1.00	−1.023	0.978
K(1)	1.00	0.989	7.450	1.012	F(4)	−1.00	−0.957	1.045
K(2)	0.62	0.633	10.564	0.979	F(5)	−1.00	−0.991	1.010
					F(6)	−1.00	−1.005	0.995
					F(7)	−1.00	−0.970	1.030
					F(8)	−1.00	−0.898	1.114
		data dispersion 0.014					data dispersion 0.056	
		sum of positive charges: 60.0					sum of negative charges: −60.0	

[a] *q* and *Q* represent the formal and the calculated charges respectively, whereas ECoN represents the equivalent coordination number. The partial occupation of the K(2) site is taken into account by multiplying the charge of the potassium cation by the occupancy factor. The fractionary *q* charge of Fe(1) comes directly from stoichiometric considerations.

feature of niobate systems, but seems to occur very frequently in ferroelectric TTB structures. Fe−F bond lengths are shown in Table 5. Despite the increased number of the independent sites in FES and of the presence of the tilt modulation, the Fe−F distances are comparable with those observed in the averaged TTB structure. Owing to the opposite displacement from the basal plane of iron and fluorine atoms, the two apical bonds are always not equivalent. The average distances involving Fe atom defining the perovskite units are comparable and close to 2.0 Å, whereas the ones related to extra-perovskite sites are shorter. As in the previous case no sure indication of charge ordering is supplied, apart from a general indication of an occupational preference of divalent Fe for the perovskite-like sites.

(c) COS Refinement. The COS structure has tetragonal symmetry, space group $P4_2bc$ and a *c* axis which is doubled with respect to the TTB cell. Structure solution and refinement has been accomplished by using fundamental reflections and COS modulation satellites; the structure has been solved ab initio with SIR2002[28] and refined with SHELX93.[27] Crystallographic data and refinement parameters are reported in Table 1 and atomic parameters are shown in Table 6. Three independent Fe sites exist in this structure, where Fe(1), Fe(2), and Fe(3) indicate the extra-perovskite and the two perovskite sites, respectively. Table 7 shows the refined Fe−F distances. The average Fe(1)−F distance is comparable (within the esd) with that found in the TTB structure. However a significant difference was found between the distances involving Fe(2) and Fe(3) sites (2.059(4) and 1.932(4) Å, respectively). By simple considerations involving the ionic radii, such distances could be related to a complete occupation of the two sites by divalent and trivalent high spin configuration Fe ions, respectively. In this hypothesis, by considering the phase stoichiometry, the extra-perovskite site Fe(1) would be occupied simultaneously by Fe^{2+} and Fe^{3+}, in agreement with its intermediate size. This results are quite similar to those found in an equivalent cell for $K_{0.54}(Mn,Fe)F_3$,[8] as expected from the similarity of the ED patterns we observed for Fe and Fe−Mn based compounds. The simple charge order model deduced by the previous considerations was checked by charge distribution analysis carried out with CHARDIS.[29] The results of the calculation are reported in Table 8 and well agree with the starting hypothesis: Fe(2) and Fe(3) show complete order between divalent and trivalent ions, while the Fe(1) charge was calculated as +2.386, in good agreement with the refined potassium amount. Figure 8 shows the charge order of the perovskite units,

(29) CHARDIS program reference: Nespolo, M.; Ferrarsi, G.; Ohashi, H. *Acta Crystallogr., Sect. B: Struct. Sci.* **1999**, *55*, 902.

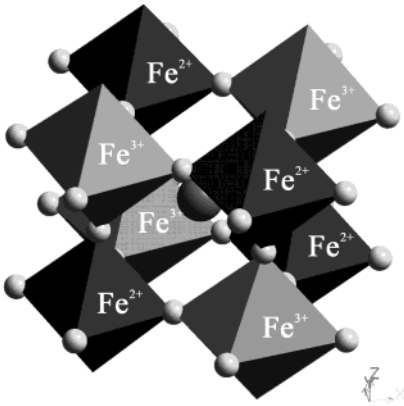

Figure 8. Charge order of the metallic cations around the perovskite cage: dark and light octahedra refer to divalent and trivalent ions, respectively.

where the different ions occupy alternate positions around the cage and along the *c* axis. The alternation of "large" and "small" octahedra minimizes the structural distortion and is responsible of the doubling of the *c* axis.

The Real Structure. The positive outcome of previous refinements shows that our starting hypothesis, to consider the modulations imposed by tilt wave and the charge order in fluoride bronzes as independent in first approximation, can be considered substantially correct. This means, on one side, that the symmetry and the amplitude of the tilt modulation, the same observed in BNN, is not strongly perturbed by the presence of octahedra of different size and, on the other side, that the stacking of "large" and "small" octahedra along *c* axis is not perturbed by their tilting directions. Therefore, since both modulations concur in the determination of the real structure, a simple model (Figure 9) can be postulated just by considering the propagation of charge ordering and tilt modulation, each one with its own symmetry and periodicity, in the real lattice. A quantitative description of the real structure, which is beyond the goal of this paper, could be achieved within the superspace approach. In theory it is possible to refine the model in a superlattice having the same periodicity of the FES structure. However the different symmetries of the two modulations force a decrease of the global symmetry to a space group, *Pbm*2, compatible with both modulations. This, in front of a small increase of the observations (the COS satellites), not only produces the doubling of the atomic sites to be refined independently (24 Fe, 18 K, 68 F) but also introduces correlation between the parameters, making the results of refinement poorly reliable.

General Considerations on the TTB Fluoride Structure. The structural information obtained by single-crystal XRD data on $K_{0.525}Fe^{II}_{0.525}Fe^{III}_{0.475}F_3$, coupled with the general information obtained by ED on different compounds, allows design of a common frame for a unified description of the structural features of the whole family of TTB fluoride bronzes.

ED patterns showed that the satellite reflections related to the tilt modulation represent a common feature of the TTB fluoride structure. Their general characteristics remain unaltered not only on the whole compositional range between $K_{0.4}MF_3$ and $K_{0.6}MF_3$, but also by changing the nature of the M cations, at least within the various compositions here presented. This suggests that the results obtained for the $K^{0.525}Fe^{II}_{0.525}$-$Fe^{III}_{0.475}F_3$ crystal could be extended to the whole family. The tilt modulation has the same features of that observed in the ferroelectric niobates, where it is related

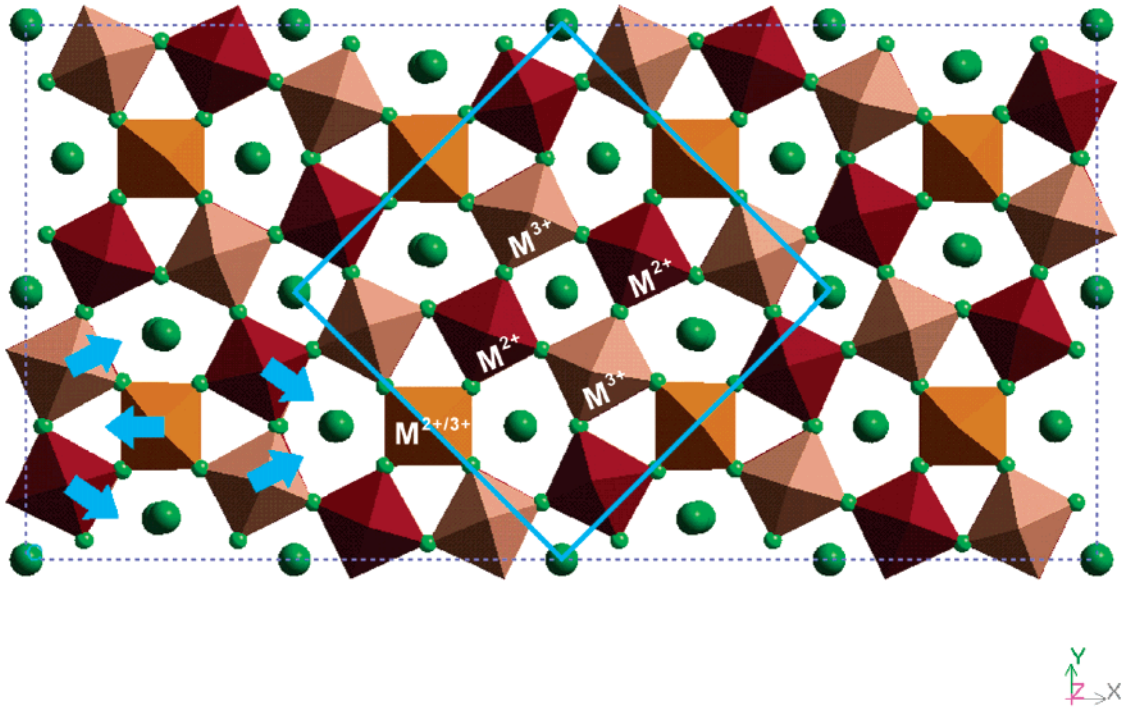

Figure 9. Model of the real structure of TTB fluorides. The color of the octahedra represents the order involving metal cations: red sites are occupied by divalent cations, brown sites are occupied by trivalent ones, and yellow sites are mixed-valence; red and brown octahedra alternate on subsequent layers, and the COS cell is delimited by the blue line. Tilting modulation, involving each octahedron, is here evidenced for only a few of them.

to their ferroelastic behavior. The main difference consists of the scale of the twinning domains, which is considerably larger in fluorides. The reason is not completely understood, even if it could be connected to the superimposition of charge order in the latter.

Concerning the ferroelectric properties in TTB fluorides, they have been reported in the literature[18,19] only in connection with the macroscopic orthorhombic distortion of the fundamental TTB cell that occurs in K_xFeF_3 for the highest values of x ($x > 0.56$). Our structural determination demonstrates that the ferroelectricity survives within the tetragonal region of the fundamental structure ($x < 0.56$) and, because of the similarities between the corresponding structures, probably extends over the whole compositional range. Preliminary refinements of the fundamental TTB structure in *P4bm* space group, performed on $K_{0.4}MF_3$ samples by XRD powder data, gave evidence of ferroelectricity with atomic displacements larger than those observed by single crystal and reported in Figure 6. The results of these refinements, despite a general good agreement with those obtained by single crystal on the TTB cell concerning the atomic distances, should be confirmed by a more accurate analysis. In fact, all the powder patterns we collected on our samples are clearly affected by microstructural effects; in particular, an asymmetric line broadening, dependent on the reciprocal lattice vector and maximum for 00*l* reflections, was observed. The *hkl*-dependent line broadening is probably related to the occurrence of polar twinning at short range, which decreases the real dimension of the crystal domains along the *c* axis. Other effects, as for example the presence of strain produced by microtwinning or a symmetry reduction related to the presence of the tilt modulation, should be responsible for the profile asymmetry. All these effects should be taken into account in the XRD powder pattern refinement for a more accurate determination of the refined parameters. Work in this direction is actually in progress.

Very interesting also is the existence of charge ordering in these compounds. From the structural point of view the occurrence of this phenomenon is usually related more to the different size of cations with different charge, rather than to the charge itself. To understand the origin of the charge ordering in our compounds, we prepared and investigated two samples of composition $K_{0.4}Fe_{0.8}In_{0.2}F_3$ and $K_{0.4}Fe_{0.4}In_{0.6}F_3$, where the magnetic ion Fe^{3+} is partially (33%) or completely substituted by the nonmagnetic ion In^{3+}, which is comparable in size to Fe^{2+}. ED patterns are shown in Figure 10, compared with that of pure iron compounds. Whereas the FES satellites persist in all patterns, the COS satellites decrease their intensity with the partial substitution and vanish for the complete one, despite the increased contrast in terms of electron density. This agrees with a completely disordered distribution of Fe^{2+} and In^{3+} in the octahedral sites of the structure. On the contrary, as long as compounds involving different cationic sizes are considered, satellites related to cationic order are observed in ED patterns.

Single-crystal data showed for $K_{0.525}FeF_3$ that cationic order, which occurs with COS periodicity and $P4_2bc$ symmetry, involves the octahedral site defining the perovskite unit. Similar results were previously found

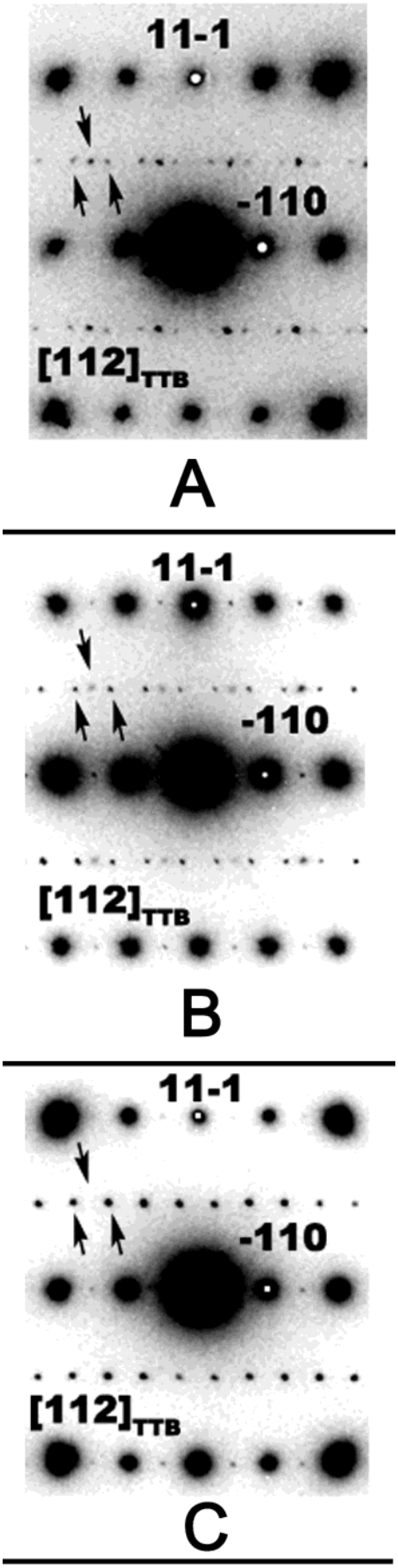

Figure 10. ED patterns of $K_{0.4}FeF_3$ (A), $K_{0.4}Fe_{0.8}In_{0.2}F_3$ (B), and $K_{0.4}Fe_{0.4}In_{0.6}F_3$ (C) taken along the same zone axis; the intensity of COS modulation satellites (downward arrows) decreases with increasing the In content.

also for $K_{0.54}(Mn,Fe)F_3$, in agreement with the strong analogy, found in this work, of the ED patterns of iron and iron−manganese compounds. Since the $P4_2bc$ symmetry is typical of all the investigated fluorides of composition $K_{0.4}MF_3$, it can be concluded that the cationic order occurs in the same way in these compounds. However, on the basis of ED data, such order should also extend to $K_{0.6}MF_3$. As pointed out in the results of TEM characterization of these compositions, the COS satellites, although breaking the extinction condition *hhl*: $l = 2n$, are nevertheless connected to the doubling of the c_{TTB} axis and therefore to a structural difference between two adjacent octahedral layers. Such extinction violation is not necessarily connected to an alteration of the charge order rules observed in $P4_2bc$ symmetry, but it could be simply imposed by an orthorhombic distortion of the unit cell that automatically removes the diagonal glide planes and reduces the symmetry to *Pba*2. This is exactly the case of $K_{0.6}FeF_3$, whose orthorhombic distortion was evident in powder XRD results, but this could likely occur also for the equivalent Mn/Fe compounds. In this case no cell distortion is directly appreciable in XRD pattern, so that even the *P*4*bm* symmetry (giving the same extinction rules of *Pba*2) should be taken into account. However, this symmetry implies the equivalence of the four M perovskite site laying at the same height *z* and is consistent with a disordered site occupation or with an occupation of the perovskite site by divalent and trivalent cations on alternate layers.

The first hypothesis is in contrast with the doubling of the c_{TTB} axis, whereas the second one, even if compatible with the composition when the extra-perovskite site is occupied by a divalent cation, should introduce structural stress and simultaneously should influence the symmetry of the FES modulation, which on the contrary remains the same. Therefore, a cationic ordering involving the perovskite sites similar to that observed in $P4_2bc$, but described by a reduced *Pba*2 symmetry, remains the more plausible hypothesis to justify the appearance of COS satellites in the $K_{0.6}MF_3$ structure.

Conclusions

A series of iron and manganese based $K_xM^{II}_xM^{III}_{1-x}F_3$ fluorides ($0.4 < x < 0.6$) showing TTB structure has been prepared by solid state reaction and characterized by XRD and ED analysis. The synergic use of these diffraction techniques evidenced unique structural features that are typical of all these materials and make them extremely interesting from the structural point of view. In fact, two distinct modulations, charge ordering and cooperative tilting involving the $[MF_6]$ octahedra of the bronze framework, coexist in the structure. Each modulation is characterized by its own symmetry and periodicity and, in first approximation, can be considered independent from the other one. Charge ordering involves the perovskite unit of the TTB structure, which is built by $[MF_6]$ octahedra in such a manner that the larger divalent cations alternate with the smaller trivalent ones to reduce the structural stress giving rise to a superstructure which is twice thevolume of the fundamental TTB cell.

The tilt modulation extends on a larger periodicity, giving rise to an orthorhombic supercell that is eight times the volume of the fundamental TTB cell. This modulation is strictly similar to that found at room temperature in ferroelectric BNN, where it is related to the appearance of ferroelasticity. On the basis of the results reported here indicating our fluorides as ferroelectric systems, such modulation seems generally distinctive of ferroelectric−ferroelastic TTB structure.

Since fluoride bronzes have already been studied for their magnetic properties originated by interactions among transition metal ions, which lead to frustrated ferrimagnetism at low temperatures, they can be considered as a promising class of multiferroic materials. Coexistence of ferroelectric and ferrimagnetic order is expected in the low temperature region, where it could also be coupled to ferroelasticity, giving rise to magnetoelectric phenomena that are actually investigated.

Supporting Information Available: X-ray crystallographic files in CIF format for structure determination of TTB, FES, and COS structures. This material is available free of charge via the Internet at http://pubs.acs.org.

CM049346P